Electronic Supplementary Material (ESI) for Journal of Materials Chemistry A.
This journal is © The Royal Society of Chemistry 2023

Electronic Supplementary Information

Epitaxial growth of single hexagonal layered α-$LiAlO_2$ coating on high-voltage $LiCoO_2$ cathode material for enhanced stability

Jiahui Zheng,[a] Yong Wang,[a] Mengmeng Qin,[a] Lidong Sun,[a] Cong Peng,[c] Yu Li*[ac] and Wei Feng*[abc]

[a] School of Material Science and Engineering and Tianjin Key Laboratory of Composite and Functional Materials, Tianjin University, Tianjin 300350, PR China
[b] Key Laboratory of Advanced Ceramics and Machining Technology, Ministry of Education, Tianjin 300354, PR China
[c] Institute of advanced technology and equipment, Beijing University of Chemical Technology, Beijing 100029, PR China
*Corresponding author
Email: weifeng@tju.edu.cn; 2022500016@buct.edu.cn

Experimental section

Preparation of Materials

In the synthesis of bare LCO, Li_2CO_3 (99%,) and Co_3O_4 (99%,) were used as raw materials and mixed (Li: Co=1.05: 1) to ball milling for 6 h, and then anhydrous ethanol was added as dispersant to obtain uniformly mixed precursor powders. Mixture was calcined at 1000 ℃ in air for 10 h and the sintered powder was fully ground, crushed and mixed again. After that, the mixture was calcined at 1000 ℃ in air for 10 h to obtain the final LCO. All commercial chemical materials were directly used without any additional treatment.

For the preparation of α-LAO on the surface of LCO, $Al(NO_3)_3 \cdot 9H_2O$ and LiOH were dissolved in deionized water (Al: Li=1: 1), and then the prepared LCO powders were added with the designed coating mass fraction. In addition, ammonium citrate was added as the complexing agent with continuous stirring at 80 ℃ until the complete evaporation of solvent, and LAO-gel coated LCO was obtained. Finally, *p*-LAO@LCO powder was sintered at 500 ℃ in air for 24 hours, with heating rate of 4 ℃/min.

Materials characterization

Ex-situ XRD data was obtained by X-ray diffractometer (Bruker D2 PHASER) with a scan rate of 1° min^{-1}, and FullProf Suite was used to get Rietveld refinement results. The appearance of pristine powders and cycled electrode were observed by scanning electron microscope (TESCAN MIRA LMS, Chech) with accelerating voltage of 15 kV. The surface compositions of pristine powders were tested by X-ray photoelectron spectrometer (ThermoFischer, ESCALAB 250XI, USA) with Al Kα X-ray (1486.6 eV) as excitation source and working voltage of 12.5 kV. The samples were thinned by Ar^+ with etching spot of 1.5mm, etching voltage of 1000 eV and etching time of 10s. Spectra were analyzed using Avantage software and adjusted all binding energy of C-C peak in C 1s spectra to 284.8 eV. The transmission electron microscope (TEM) images were gained from FEI Talos F200XG2 AEMC. The finer lattice structure on particle surface was investigated using Titan Cubed Themis G2300 with a probe spherical aberration corrector at 300 kV to acquire STEM-HAADF and EDS images. In-situ XRD test was carried on Bruker D8 Advance ECO with special in-situ test accessories. As for characterizations of cycled electrode or powders, the cycled cells were disassembled in argon atmosphere of glove box with moisture/oxygen contents below 0.1 ppm, and acquired cathode sheets were washed with DEC at least three times.

The Al and Co atomic ratios of *g*-LAO@LCO and LAO@LCO at different etching depths was based on data of etching times, and the calculation process is as follows:

Theoretically, the detection depth of XPS test is 10 nm and the etching depth for the alternated Ar ion etching process is 2 nm. The Al atomic ratios directly obtained from the XPS depth profiles are setted as X_0, X_1, X_2, X_3, X_4, X_5 along with the etching time, respectively. Then, the Al atomic ratios of etching depth in the range of 0~2, 2~4, 4~6, 6~8, and 8~10 nm were settled as x_1, x_2, x_3, x_4, and x_5, respectively. So, the Al atomic ratios of etching depth in the range of 10~12, 12~14, 14~16, 16~18, and 18~20 nm were x_5-v, x_5-2v, x_5-3v, x_5-4v, and x_5-5v, respectively. These parameters were in accordance with the following equations:

$(x_1+x_2+x_3+x_4+x_5)/5=X_0$;

$(x_2+x_3+x_4+x_5+x_5\text{-}v)/5=X_1$;

$(x_3+x_4+x_5+x_5\text{-}v+x_5\text{-}2v)/5=X_2$;

$(x_4+x_5+x_5\text{-}v+x_5\text{-}2v+x_5\text{-}3v)/5=X_3$;

$(x_5+x_5\text{-}v+x_5\text{-}2v+x_5\text{-}3v+x_5\text{-}4v)/5=X_4$;

$(x_5\text{-}v+x_5\text{-}2v+x_5\text{-}3v+x_5\text{-}4v+x_5\text{-}5v)/5=X_5$;

Therefore, the Al atomic ratios in different etching depths can be obtained by solving these equations, and the Co atomic ratios could be calculated through the same process.

Electrochemical measurements

Half-cell (CR2032-coin cells) was made to evaluate the electrochemical performance of LCO and manufactured compounds in a glove box filled argon atmosphere, using separator (Celgard 2325) as separator, metal lithium sheet as anode, and 50 μl electrolyte of 1.0 M $LiPF_6$ dissolved in EC/DEC (1: 1 in vol) with 5.0 vol% FEC additive. For the preparsion of cathode plate, N-methyl pyrrolidone (NMP) was used as solvent with 80 wt% active material, 10 wt% poly (vinylidene difluoride) (PVDF) as binder and 10 wt% conductive carbon black, which was fully mixed and grounded to form a uniform slurry. Then, the slurry was uniformly coated on the Al foil, drying in vacuum at 120 ℃ for 16 h and cutting into circular disks with the diameter of 12 mm. The average loading amount of active material on the cathode plate was 5~8 mg cm^{-2}.

The galvanostatic charge-discharge measurements of fabricated half-cells were tested with the voltage range of 3.0 V~4.6 V or 3.0 V~4.65 V at room temperature on the LAND test system (CT3002A, Wuhan, China). In the rate capacity test, the rates increased gradually including 0.1C, 0.2C, 0.5C, 1C, 2C, 5C and 10C (1C=274 mAh g^{-1}). In the GITT test, cells were relaxed for 0.5 h after each 200 s of charge and discharge at the rate of 0.5C. The CV test of five cycles was 3.0 v~4.6 V with scanning rate of 0.1 mV s^{-1} on electrochemical station (ZAHNER Zennium Pro). EIS was carried out on the same electrochemical station in the frequency range of 8 MHz~100 mHz with a

potential amplitude of 10 mV.

Theoretical calculation

All the spin-polarized DFT calculations were conducted based on the Vienna Ab-inito Simulation Package (VASP) [1, 2]. The electron-ion interactions were described by the Projected Augmented-Wave (PAW) potentials, while the exchange-correlation interactions were calculated by employing the Perdew-Burke-Enzerhof (PBE) pseudopotentials of Generalized Gradient Approximation (GGA) [3, 4] with a Hubbard U extension (U value) of 3.32 eV for Co. The vdW-D3 method developed by Grimme was employed to describe the van der Waals interaction [5]. The plane-wave energy cutoff was set as 520 eV. The convergence threshold was set as 1.0×10-6 eV in energy and 0.02 eV per Angstrom in force. Firstly, $LiCoO_2$, α-$LiAlO_2$ and β-$LiAlO_2$ bulk geometry relaxation were performed. Then, the heterojunction consisting of p(1×1) of $LiCoO_2$(010) and p(1×1) of α-$LiAlO_2$(010) was built. The heterojunction consisting of p(1×4) of $LiCoO_2$(010) and p(3×2) of β-$LiAlO_2$(010) was built. The Brillouin zone was modeled by gamma centered Monkhorst-Pack scheme, in which 2×9×2 and 1×1×1 grids were adopted for α-$LiAlO_2$@$LiCoO_2$ and β-$LiAlO_2$@$LiCoO_2$, respectively.

The plane-wave energy cutoff was set as 400 eV and 4×4×1 $LiCoO_2$ and α-$LiAlO_2$ supercell were built and geometry relaxation were performed. Then, 80% Li atoms of $LiCoO_2$ were randomly removed. Furthermore, 20% Co atoms of the last configuration were replaced by Al. The Brillouin zone was modeled by gamma centered Monkhorst-Pack scheme, in which a 1×1×1 grid was adopted for all supercell models.

Figures

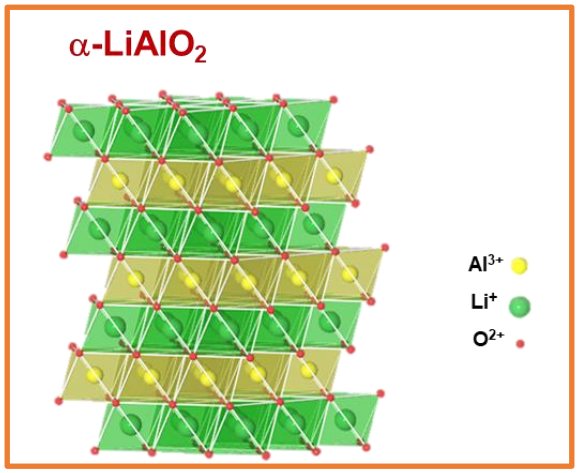

Figure S1 Schematic diagram of crystal structure of α-LAO

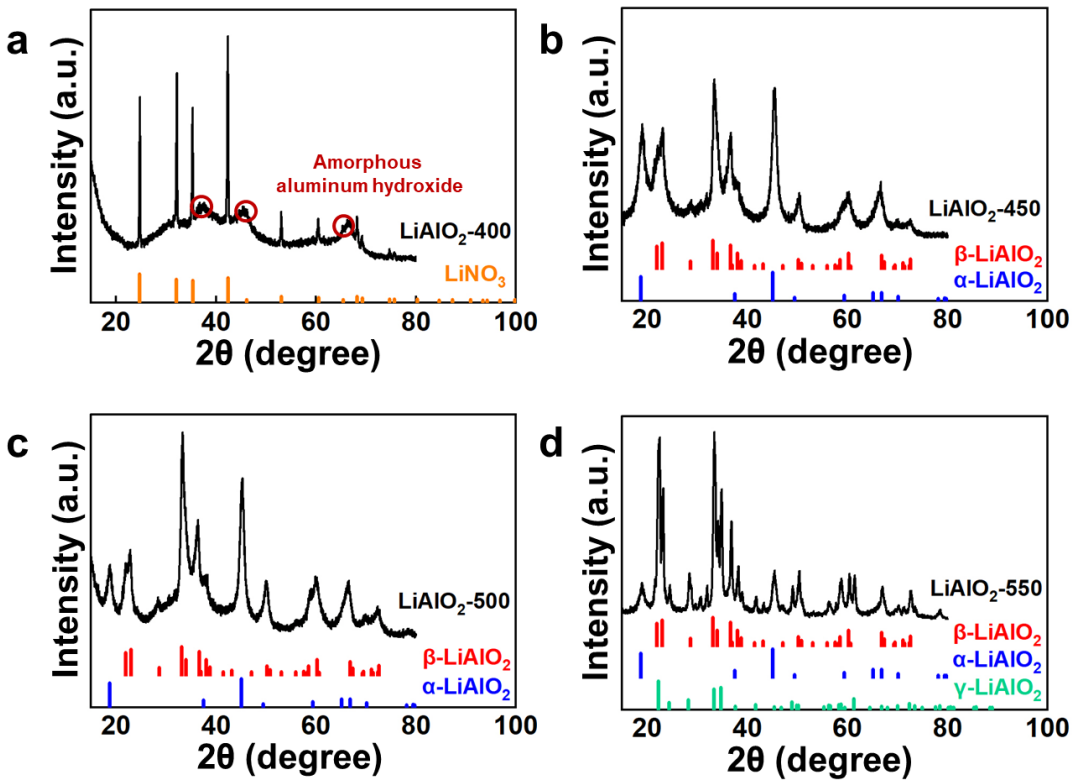

Figure S2 XRD patterns of LAO powder calcinated at (a) 400 ℃, (b) 450℃, (c) 500℃ and (d) 550℃, respectively.

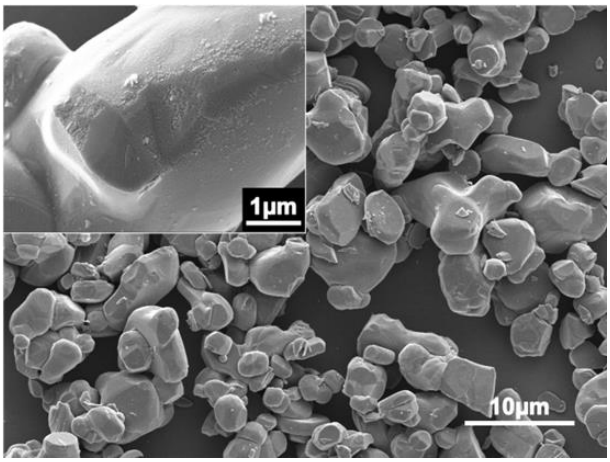

Figure S3 SEM images of *p*-LAO@LCO and the inset is the magnificated SEM image for a single *p*-LAO@LCO particle.

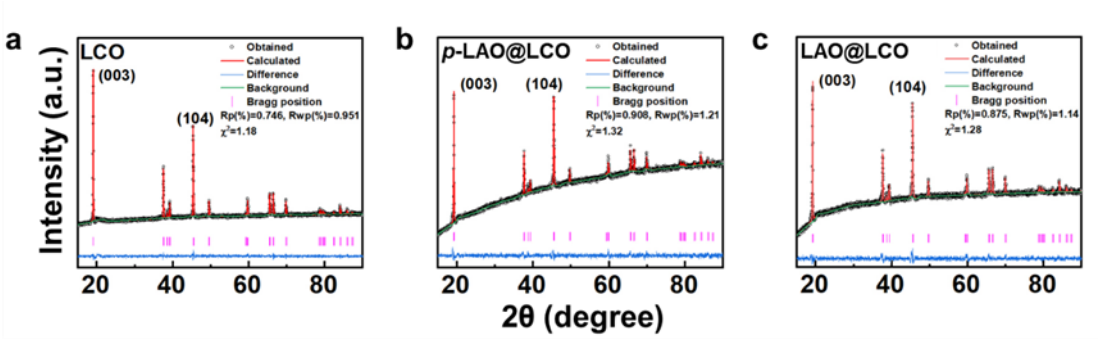

Figure S4 Rietveld-refined XRD patterns of (a) LCO, (b) *p*-LAO@LCO and (c) LAO@LCO, respective.

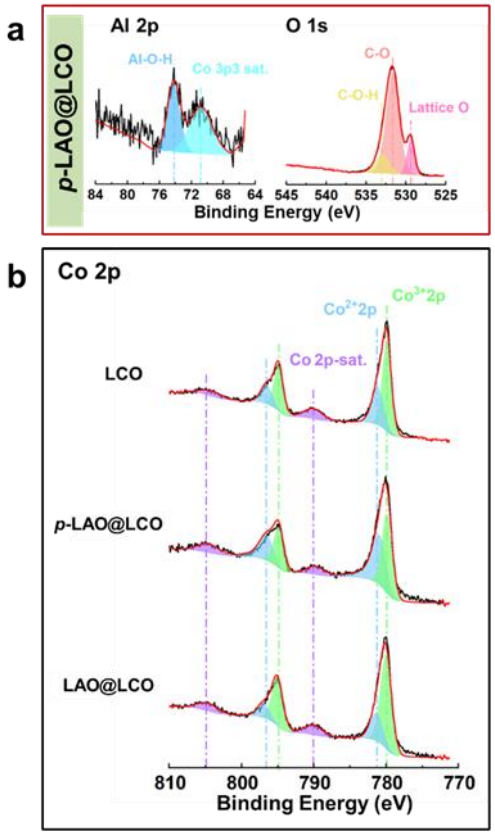

Figure S5 (a) XPS spectra of Al 2p and O 1s core level from *p*-LAO@LCO; (b) Co 2p XPS spectra of LCO, *p*-LAO-LCO and LAO@LCO.

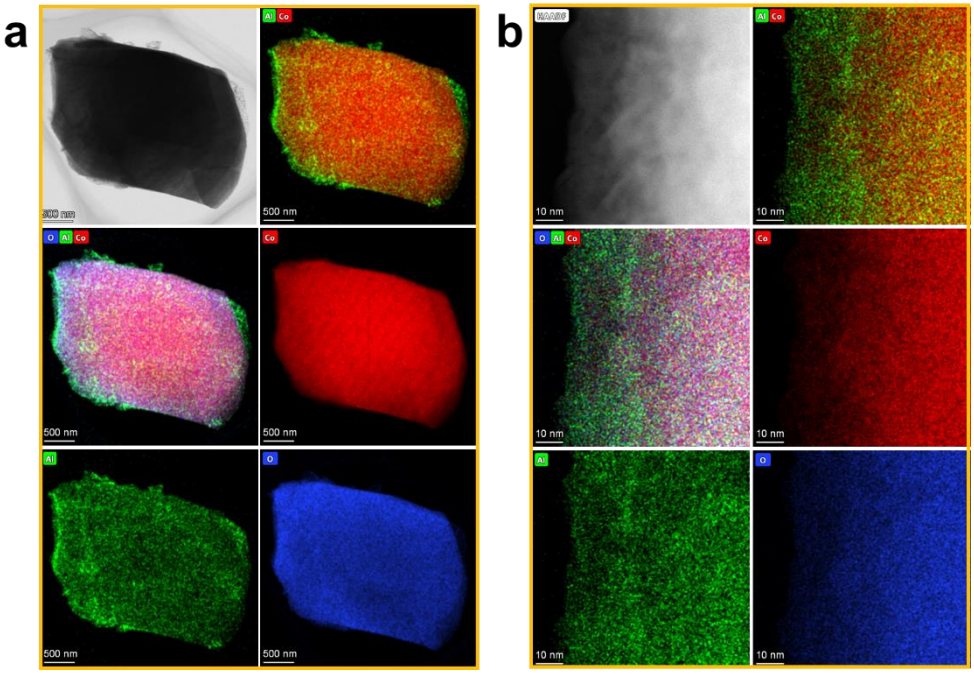

Figure S6 EDS mapping of LAO@LCO particle at (a) low and (b) high magnification.

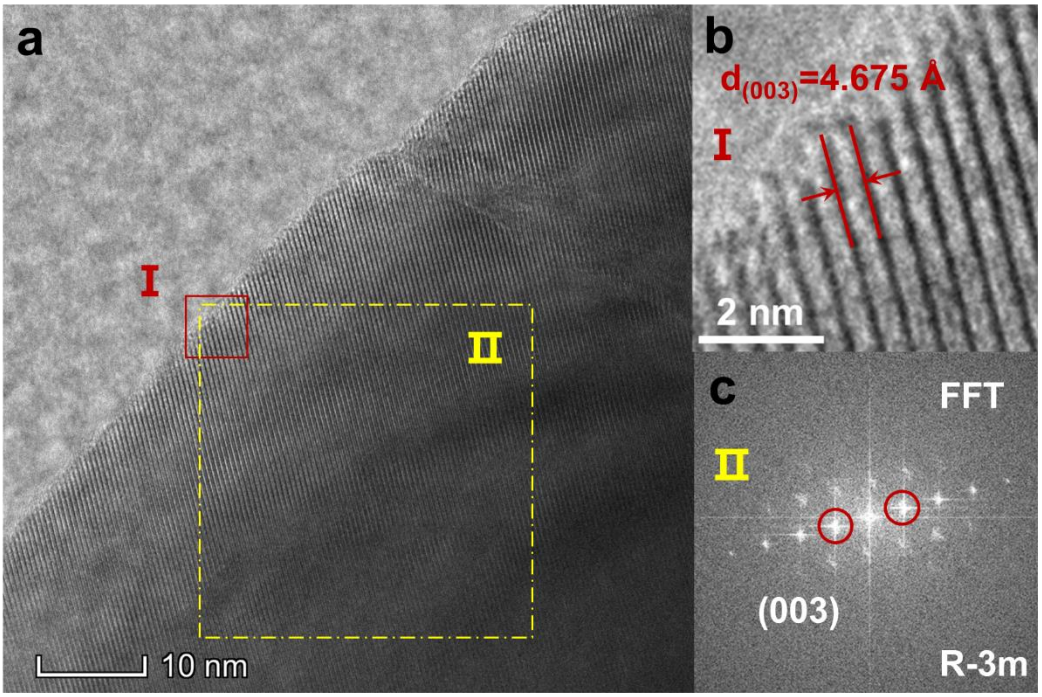

Figure S7 HRTEM image (a) of LCO and the magnificated HRTEM image (b) of the framed area labelled I and corresponding FFT pattern (c) of the framed area labelled II.

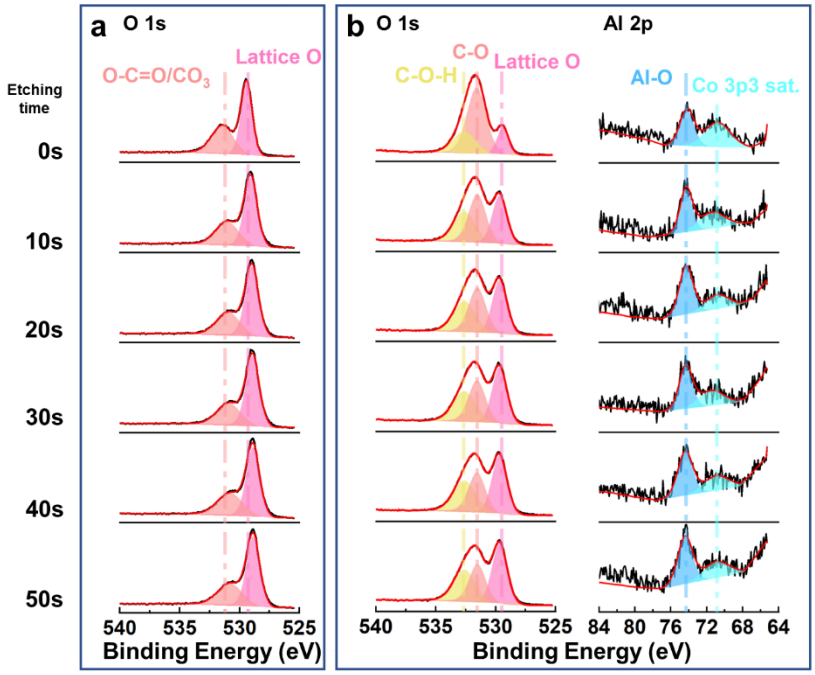

Figure S8 XPS spectra of O1s and Al 2p core levels from (a) LCO and (b) *p*-LAO@LCO by XPS depth profiles.

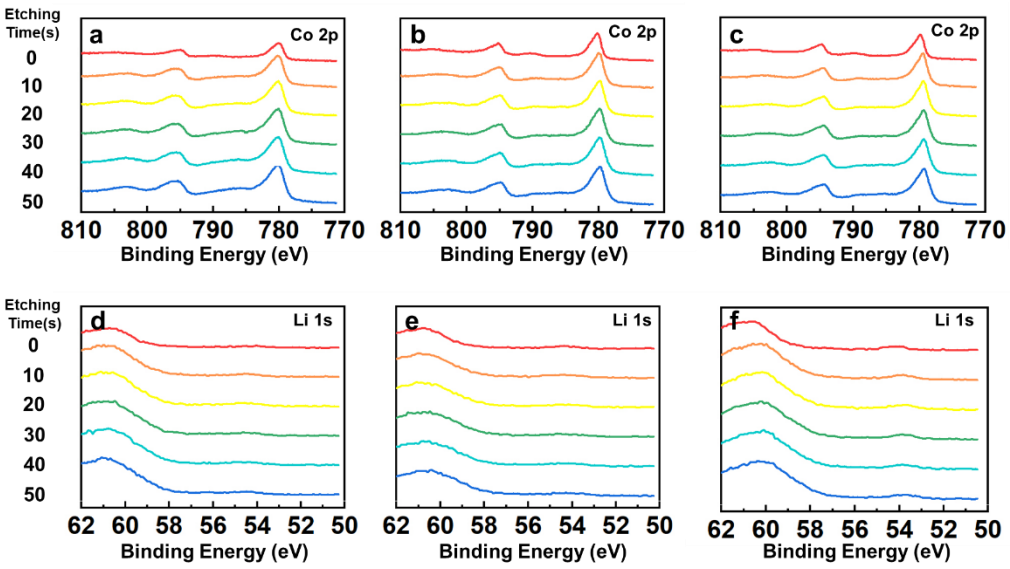

Figure S9 XPS spectra of Co 2p and Li 1s core levels from (a, d) LCO, (b, e) *p*-LAO@LCO and (c, f) LAO@LCO by XPS depth profiles.

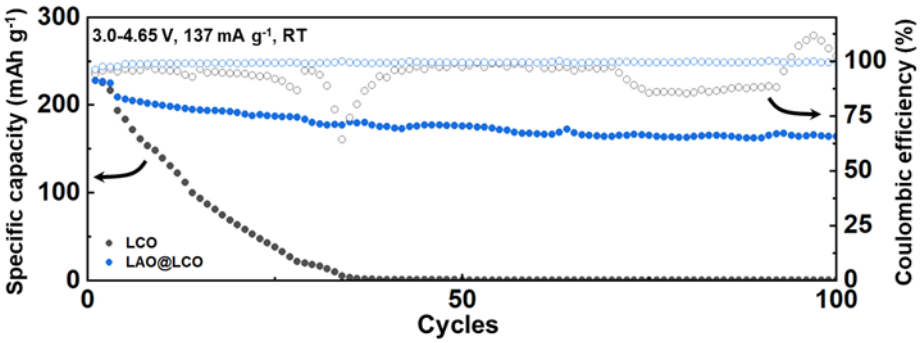

Figure S10 Cyclic performance of LCO and LAO@LCO at 0.5C in the range of 3.0-4.65 V after the initial three cycles at 0.1C.

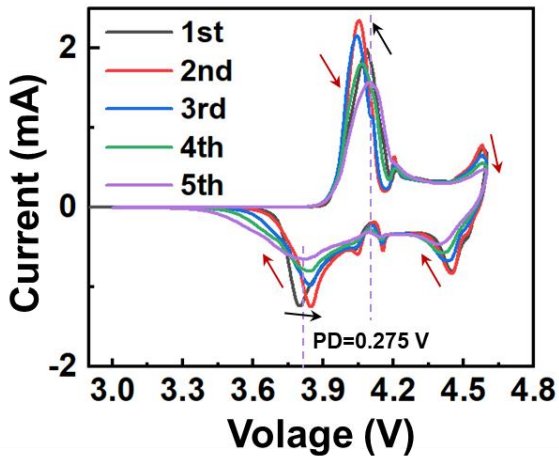

Figure S11 CV curves of LCO at the scan rate of 0.1 mV s^{-1} in the voltage range of 3.0-4.6 V (vs Li/Li^+).

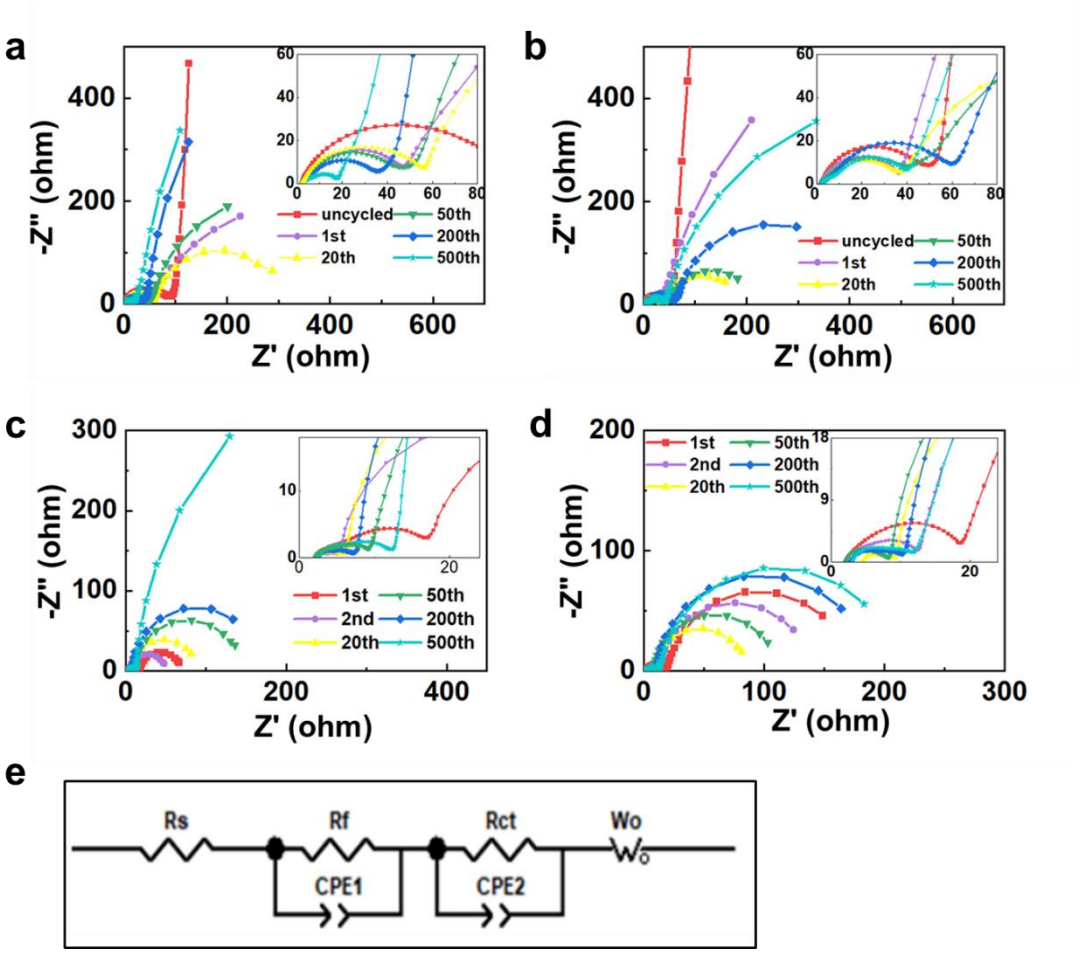

Figure S12 Nyquist curves of (a, c) LCO and (b, d) LAO@LCO after different cycles at (a, b) fully discharged and (c, d) charged states; (e) Equivalent circuit diagram.

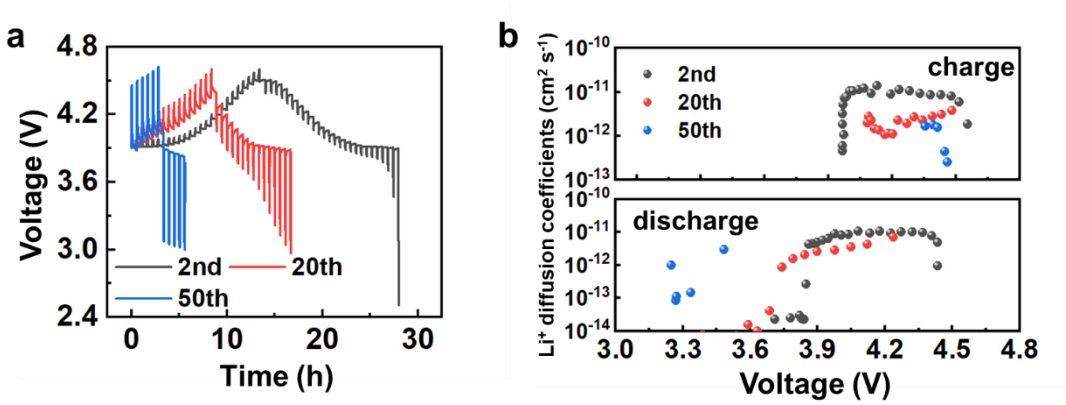

Figure S13 GITT curve of (a) bare LCO and corresponding (b) Li^+ diffusion coefficient.

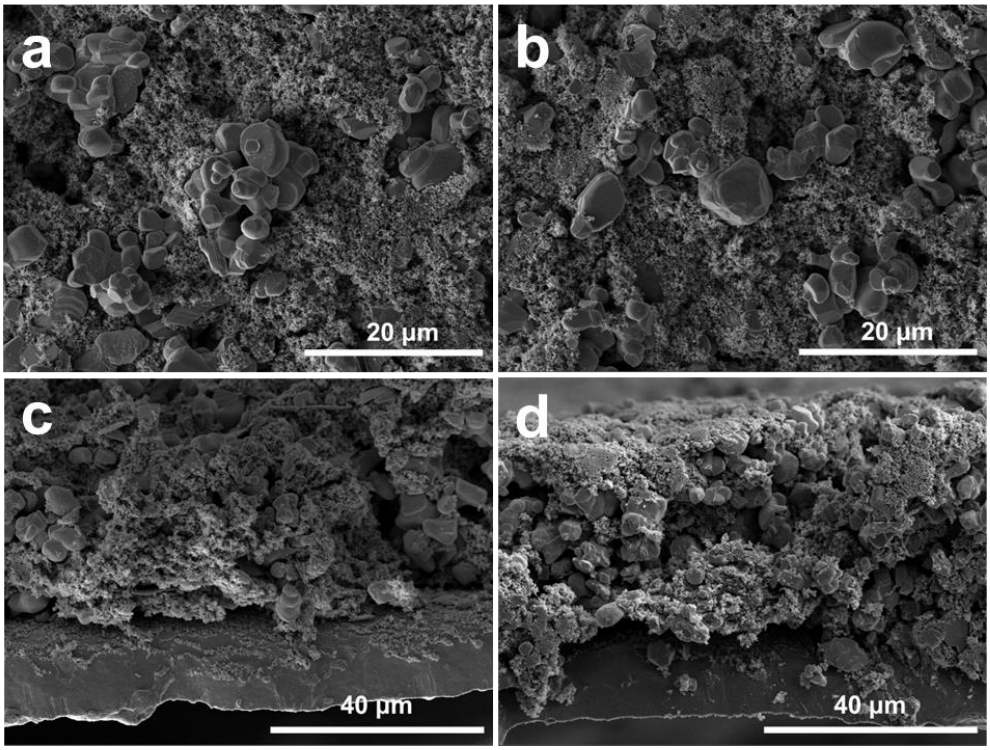

Figure S14 SEM images of (a, b) surface and (c, d) cross-section of pristine (a, c) LCO and (b, d) LAO@LCO electrodes.

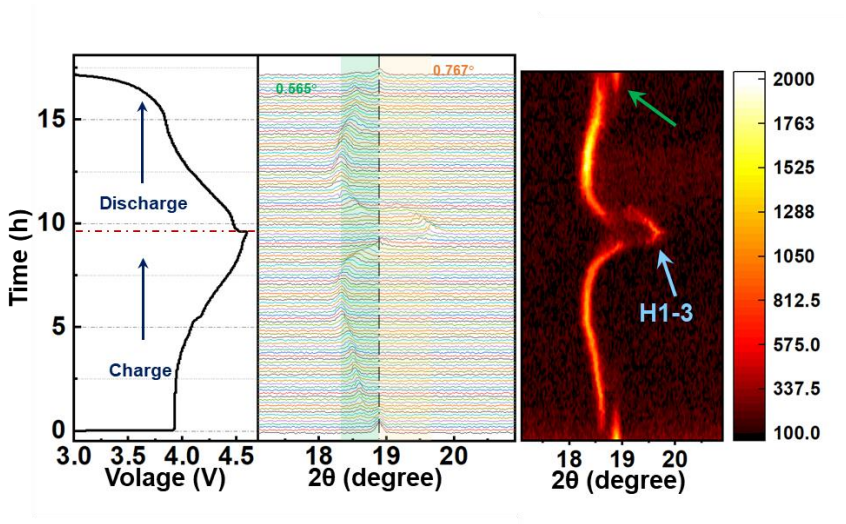

Figure S15 In-situ XRD evolution of LCO electrode during the initial charge-discharge cycle.

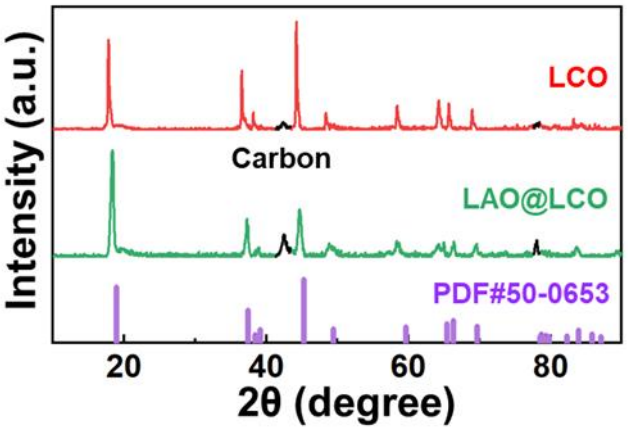

Figure S16 XRD patterns of (a) LCO and (b) LAO@LCO electrodes after 300 cycles at 0.5C.

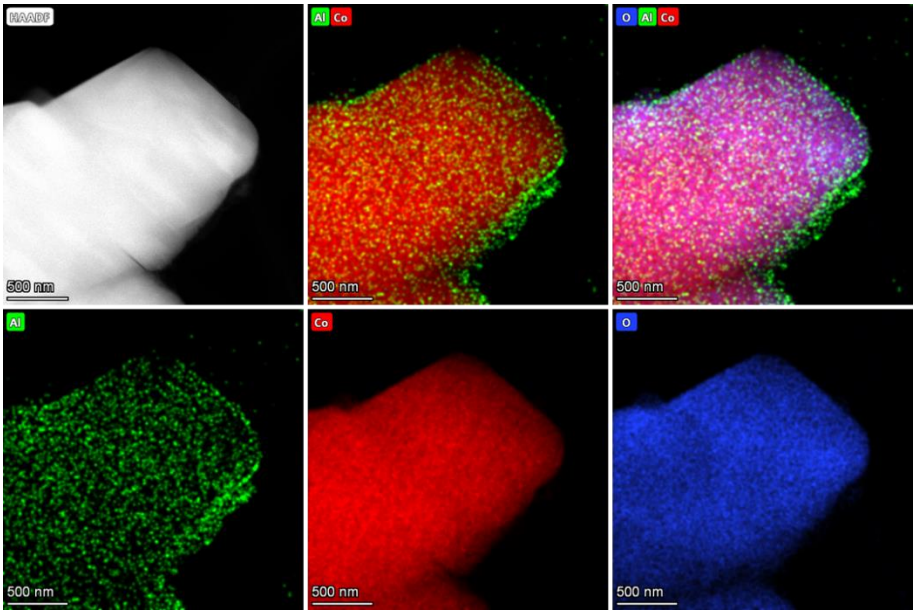

Figure S17 EDS mapping of the cycled LAO@LCO.

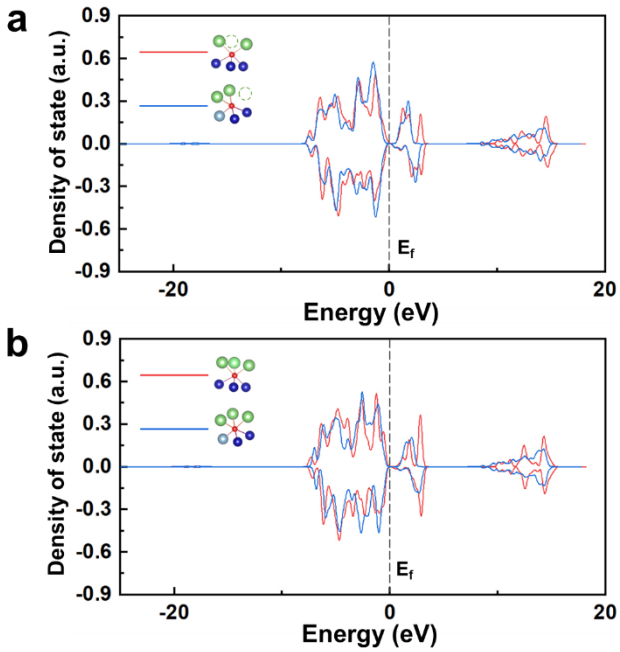

Figure S18 PDOS of different O-2p with (a) one or (b) zero vacancy in LCO bulk and doping layer.

Tables

Table S1 The low-index crystal planes of LCO and β-LAO.

	Crystal plane	U(Å)	V(Å)	α(degree)
$LiCoO_2$	100	11.26164	14.05088	90.000
	010	14.05088	11.26164	90.000
	001	11.26164	11.26164	120.000
	110	14.05088	19.50573	90.000
	101	18.00699	11.26164	108.22213
	011	11.26164	18.00699	108.22213
	111	18.00699	18.00699	65.58736
	104	41.46470	11.26164	90.000
β-$LiAlO_2$	100	12.600	14.700	90.00000
	010	14.700	10.560	90.00000
	001	10.560	12.600	90.00000
	110	14.700	16.440	90.00000
	101	18.099823	12.60000	90.00000
	011	10.560	19.36104	90.00000
	111	16.440	18.09982	67.99060
	104	44.724798	12.60000	90.00000

Table S2 The difference between R-3m (010) crystal plane and Pna21 (010) crystal plane.

	U(Å)	V(Å)	α(degree)	Area($Å^2$)	%U	%V	%α	%Area
$LiCoO_2$(010)	14.051	11.262	90	158.242	4.61	6.2	0	1.9
β-$LiAlO_2$(010)	14.700	10.560	90	155.232				

Table S3 Rietveld refinement results of XRD of LCO, *p*-LAO@LCO and LAO@LCO.

Samples	a (Å)	c (Å)	V ($Å^3$)	Rp (%)	χ^2	c%
LCO	2.81518	14.05396	96.459	0.746	1.18	0
***p*-LAO@LCO**	2.81524	14.05288	96.455	0.908	1.32	-0.007
LAO@LCO	2.81496	14.05709	96.465	0.875	1.28	0.022

Table S4 The results of impedance values of LCO and LAO@LCO after different cycles.

	Number of cycles	Discharge state			Charge to 4.6 V		
		R_e/Ω	R_{cei}/Ω	R_{ct}/Ω	R_e/Ω	R_{cei}/Ω	R_{ct}/Ω
LCO	**Pristine**	1.122		86.04	2.009	18.14	47.96
	1st	2.314	46.03	551.8	2.142	3.562	43.54
	20th	2.264	53.19	264.7	2.167	4.276	82.28
	50th	2.313	47.32	600.9	1.982	7.989	137.1
	200th	2.343	37.82	4006	2.125	5.747	165.9
	500th	2.267	17.19	7400	2.107	11.06	986.5
LAO@LCO	**Pristine**	2.139		44.52	2.004	17.66	156.5
	1st	1.680	35.96	1480	1.772	11.56	125.1
	20th	2.367	35.42	154.9	4.167	5.259	76.06
	50th	2.010	42.58	190.1	1.958	6.332	103.6
	200th	2.541	65.82	337.0	2.296	8.562	175.7
	500th	2.574	45.24	826.8	2.462	10.17	205.0

Table S5 The summarization of area and ratio of different sections in PDOS of various O-2p.

State of oxygen	Total area	Above E_f		0~5 eV	
		Area	%Area	Area	%Area
O-3Co3V_{Li}	4.52670	1.14353	0.25262	0.7867	0.17379
O-3Co1Li2V_{Li}	4.54483	1.10640	0.24344	0.67597	0.14873
O-2Co1Al1Li2V_{Li}	4.44694	0.96716	0.21749	0.50846	0.11434
O-3Al3Li	4.37159	0.76264	0.17445	0	0
O-3Co3Li	4.62180	1.12521	0.24346	0.52387	0.11335
O-2Co1Al3Li	4.53946	1.01229	0.22300	0.39559	0.08714
O-3Co2Li1V_{Li}	4.61251	1.15226	0.24981	0.61283	0.13286
O-2Co1Al2Li1V_{Li}	4.54305	1.04455	0.22992	0.46486	0.10232

Table S6 Summary of electrochemical properties of the modified LCO with different interface coating containing Al at the high cutoff voltage.

strategy	Initial capacity (mAh g^{-1}) (Cycle rate)	Final capacity (mAh g^{-1}) (Cycle number)	Capacity retention (%)	Voltage range (V *vs.* Li/Li+)	Ref.
La, Al doped LCO	190(0.1C) 181.3(C/3)	174(50)	96	3.0~4.5	[6]
Ti, Mg, Al doped LCO	219.1(0.1C) 202.3(0.5C)	174(100)	86	3.0~4.6	[7]
Al-oxide coated LCO	257(0.05C) 247(0.2C)	204(20)	82.6	3.0~4.7	[8]
AlZnO coated LCO	205(0.1C) 183.9(0.5C)	150(100) 120.8(500)	81.6 65.7	3.0~4.6	[9]
LATP coated LCO	214.6(0.2C) 204.2(0.5C)	180.3(100)	88.3	3.0~4.6	[10]
$Li_4Ti_5O_{12}$ coated ang Al doped LCO	180.4(0.5C)	156.4(100)	86.7	3.0~4.5	[11]
LAP coated LCO	214.1(0.1C) 203.6(0.5C)	190.5(100) 180.4(200)	93.6 88.6	3.0~4.6	[12]
$LiMO_2$(M: Co, Al, Zr) coated LCO	228(0.05C) 213(1C)	189(100)	88.8	2.5~4.6	[13]
$LiCo_{1-x}Al_xO_2$, $LiAlO_2$ coated LCO	178.1(1C)	170.5(100) 130.0(500)	95.7 73	3.0~4.5	[14]
$LiAlO_2/Al_2O_3$-coated nano-$LiCoO_2$	225(0.1C) 156.1(3C)	128(425)	82	3.0~4.6	[15]
$LiAlO_2$ layers by ALD	218.8(0.1C)	172.2(50)	78.7	2.75~4.6	[16]
This work: α-$LiAlO_2$ coated LCO	218.6(0.1C) 202.7(0.5C)	191.5(100) 158.8(300)	94.5 78.3	3.0~4.6	

References

[1] G. Kresse and J. Furthmüller, *Comp. Mater. Sci.*, 1996, **6**, 15-50.

[2] G. Kresse and J. Furthmüller, *Phys. Rev. B.*, 1996, **54**, 11169-11186.

[3] P. E. Blöchl, *Phys. Rev. B.*, 1994, **50**, 17953-17979.

[4] J. P. Perdew, K. Burke and M. Ernzerhof, *Phys. Rev. Lett.*, 1997, **78**, 1396-1396.

[5] S. Grimme, J. Antony, and S. Ehrlich, *J. Chem. Phys.*, 2010, **132**, 154104.

[6] Q. Liu, X. Su, D. Lei, Y. Qin, J. G. Wen, F. M. Guo, Y. M. A. Wu, Y. C. Rong, R. H. Kou, X. H. Xiao, F. Aguesse, J. Bareno, Y. Ren, W. Q. Lu, Y. X. Li, *Nat. Energy,* 2018, **3**, 936-943.

[7] J. N. Zhang, Q. H. Li, C. Y. Ouyang, X. Q. Yu, M. Y. Ge, X. J. Huang, E. Y. Hu, C. Ma, S. F. Li, R. J. Xiao, W. L. Yang, Y. Chu, Y. J. Liu, H. G. Yu, X. Q. Yang, X. J. Huang, L. Q. Chen, H. Li, *Nat. Energy*, 2019, **4**, 594-603.

[8] A. Yano, M. Shikano, A. Ueda, H. Sakaebe, Z. Ogumi, *J. Electrochem. Soc.*, 2017, **164**, A6116-A6122.

[9] X. R. Yang, M. Lin, G. R. Zheng, J. Wu, X. S. Wang, F. C. Ren, W. G. Zhang, Y. Liao, W. M. Zhao, Z. R. Zhang, N. B. Xu, W. L. Yang, Y. Yang, *Adv. Funct. Mater.*, 2020, **30**, 2004664.

[10] Y. Wang, Q. H. Zhang, Z. C. Xue, L. F. Yang, J. Y. Wang, F. Q. Meng, Q. H. Li, H. Y. Pan, J. N. Zhang, Z. Jiang, W. L. Yang, X. Q. Yu, L. Gu, H. Li, *Adv. Energy Mater.*, 2020, **10**, 2001413.

[11] C. W. Wang, Y. Zhou, J. H. You, J. D. Chen, Z. Zhang, S. J. Zhang, C. G. Shi, W. D. Zhang, M. H. Zou, Y. Yu, J. T. Li, L. Y. Zeng, L. Huang, S. G. Sun, *Acs Appl. Energ. Mater.*, 2020, **3**, 2593-2603.

[12] X. Wang, Q. Wu, S. Y. Li, Z. M. Tong, D. Wang, H. L. L. Zhuang, X. Y. Wang, Y. Y. Lu, *Energy Storage Mater*., 2021, **37**, 67-76.

[13] A. Yano, N. Taguchi, H. Kanzaki, M. Shikano, H. Sakaebe, *J. Electrochem. Soc.*, 2021, **168**, 050517.

[14] L. Shao, L. Zhou, L. S. Yang, C. K. Jia, C. H. Wang, S. Hu, X. F. Zeng, C. M. Yang, C. H. Huang, Y. Y. Zhou, X. M. Xi, *Electrochimica Acta*, 2019, **297**, 742-748.

[15] C. L. Chen, W. L. Yao, Q. R. He, M. Ashuri, J. Kaduk, Y. Z. Liu, L. Shaw, *Acs Appl. Energ. Mater.*, 2019, **2**, 3098-3113.

[16] J. Xie, J. Zhao, Y. Y. Liu, H. T. Wang, C. Liu, T. Wu, P. C. Hsu, D. C. Lin, Y. Jin, Y. Cui, *Nano Res.*, 2017, **10**, 3754-3764.